Coherent and Turbulent Process Analysis in the Flow past a Circular Cylinder at High Reynolds Number

R. PERRIN[1,2], M. BRAZA[1], E. CID[1], S. CAZIN[1], P. CHASSAING[1], C. MOCKETT[2], T. REIMANN[2], F. THIELE[2]

[1] *Institut de Mécanique des Fluides de Toulouse, Unité Mixte C.N.R.S.-I.N.P.T. 5502, Av. du Prof. Camille Soula, 31400 Toulouse, France*

[2] *Institut für Strömungsmechanik un Technische Akustik, TU-Berlin, Müller Breslau Str. 8, 10623 Berlin, Germany*

Abstract. With the aim of providing a database useful for validation and improvement of turbulence models for strongly detached flows, the flow past a circular cylinder at high Reynolds number has been experimentally studied using PIV, stereoscopic PIV and Time Resolved PIV in the very near wake. As the presence of coherent structures and their non linear interactions with the turbulent motion have to be taken into account in a model, a particular attention was paid to the decomposition of the flow into a coherent and a turbulent part. This was achieved using phase averaging and also using Proper Orthogonal Decomposition. In a precedent study, it was found that the POD coefficients could be used to define a phase angle representative of the vortex shedding, and that defining the phase angle from the POD coefficients may alleviate the overestimation of the turbulent stresses due to phase jitter between the trigger signal and the velocity, compared to a definition of the phase angle from a wall pressure time trace. In this paper two new complementary data sets, which are resolved in time and space, are analysed with the objectives of, first, providing an evaluation of the performed conditional averaging and, second, to achieve a more complete description of the flow. The main results presented here are issued from Time Resolved PIV measurements which were carried out in the near wake. Some results of a Detached Eddy Simulation which have been validated against experiment, are also used.

Key words: Cylinder wake, phase averaging, POD, Time Resolved PIV, DES.

1. Introduction

Modelling and simulating unsteady turbulent flows past bluff bodies remains a very challenging task, given the strong separations, and the presence of coherent structures in non linear interactions with the turbulent motion, which have to be taken into account in the model used. A experimental data base concerning this class of flow, which can be used for validation or improvement of modelling, is therefore of significant relevance. In this study, the generic case of a circular cylinder was chosen, first because of the strong separations and the presence of coherent structures, and also, because of the symmetries of the flow, which allow adapted processing, and then a better visualisation of the flow. With the aim of allowing direct comparison possible with simulations, and therefore evaluations of the models themselves, the cylinder was placed in a confined environment (a square channel) with a high blockage coefficient and a low aspect ratio, thereby allowing simulations to be made on a

domain of moderate size, corresponding to the experimental geometry, with the use of well defined boundary conditions.
In precedent studies, the data base was achieved using pressure measurements, PIV, stereoscopic PIV and Time Resolved PIV, carried out near the separation and in the very near wake of the cylinder, [10]. The main limitation concerning the TRPIV measurements was the size of the domain which was smaller than that of the low data rate acquisitions, due to the low energy of the laser used. A particular attention was paid to the decomposition of the flow into a coherent part and a turbulent part. To this purpose, phase averaging, using pressure on the cylinder as a reference signal, and POD have been first applied and compared. Both decompositions have been analysed with the help of TRPIV measurements in the small domain, by comparing the contributions of coherent and turbulent fluctuations to the mean Reynolds stress tensor. It has been found, in agreement with many other studies (e.g. [1]), that phase averaging with pressure leads to an overestimation of the turbulent motion and a smoothing of the Kármán vortices, resulting from phase lags occurring at certain instants between the pressure signal and the velocity to be averaged in the wake. On the other hand, POD was found useful to analyse the different parts of the flow, but the main difficulty lies in the choice of the modes to reconstruct the coherent motion. An enhancement of the phase averaging was then achieved, using a definition of the phase angle based on the first two POD coefficients, and thereby alleviating the phase lags effects as the phase is determined directly from the velocity fields to be averaged. This phase averaging was obtained from low data rate PIV.
Two new complementary data sets are analysed in this study. First, Time Resolved PIV measurements have been carried out in a domain of similar size as that of the low data rate PIV, using a cylinder of smaller physical size and a laser delivering more energy. Also, a Detached Eddy Simulation has been performed on a domain which corresponds precisely to the experiment. Then, the objectives of this study is both, to use these data resolved in space and time to evaluate the performed conditional averaging, and to achieve a better analysis of the flow.
Section 2. briefly presents the configuration of the flow and the new measurements which were carried out, together which some comparisons whith previous measurements. In section 3., the instantaneous motion is analysed. Section 4. is devoted to the analysis of POD and phase averaging. Finally an analysis of coherent and incoherent quantities is conducted in section 5..

2. Configuration and experimental set-up

The experiments were conducted in the wind tunnels S1 and S4 of IMFT. As mentioned in the preceding section, a high blockage coefficient and a low aspect ratio were employed to allow comparison with simulations carried out on a domain corresponding precisely to the experimental geometry without the use of 'infinite boundary conditions'. For the previous measurements, the cylinder had a diameter of 14cm and was placed in a square channel of cross section 67×67 cm, leading to a blockage coefficient of D/H=0.21 and an aspect ratio of L/D=4.8. Due to the low energy of the laser used, and to the access of the wind tunnel, the previous TRPIV measurements were limited to a small domain. To carry out TRPIV on a larger domain in the wake, the new measurements have been done in the wind tunnel S4 of IMFT, which has a cross section of 61×71cm. To keep the same blockage coefficient

as in the previous measurement, the diameter of the cylinder was chosen 12.5cm, which results in a blockage coefficient of 0.21 and an aspect ratio of 5.7. Although this aspect ratio is different from the previous one and therefore the flow was not expected to be rigourously the same, it will be shown that a good agreement with the old measurements is achieved for the mean flow and the velocity spectra.

A detailled description of the former measurements by low data rate PIV can be found in [11], as well as the procedure used for the reconstruction of the three components in stereoscopic measurements. The new measurements were done using a laser Darwin 2 × 20 mJ from Excel Technology, a camera CMOS APX (PHOTRON) with a resolution of 1024x1024 pixels, and DEHS as seeding particles (typical size 1μm). The system allowed acquisition of image pairs at a rate of 1kHz. The image pairs were analysed using an in-house code 'PIVIS' developed by the 'Services Signaux Images' of IMFT, which uses an algorithm based on a 2D FFT cross correlation function implemented in an iterative scheme with a sub-pixel image deformation ([5]). The flow was analysed by cross-correlating 50% overlapping windows of 32x32pixels, yielding fields of 61x57 vectors with a spatial resolution of 3mm (0.0238D). Approximately 2% of the calculated vectors were detected as outliers using a sort based on the norm, the signal-to-noise ratio, and a median test filter, and these vectors were replaced using a second order least square interpolation scheme. Six temporal series of 3072 images pairs have been acquired and analysed, each series containing approximately 85 vortex shedding periods.

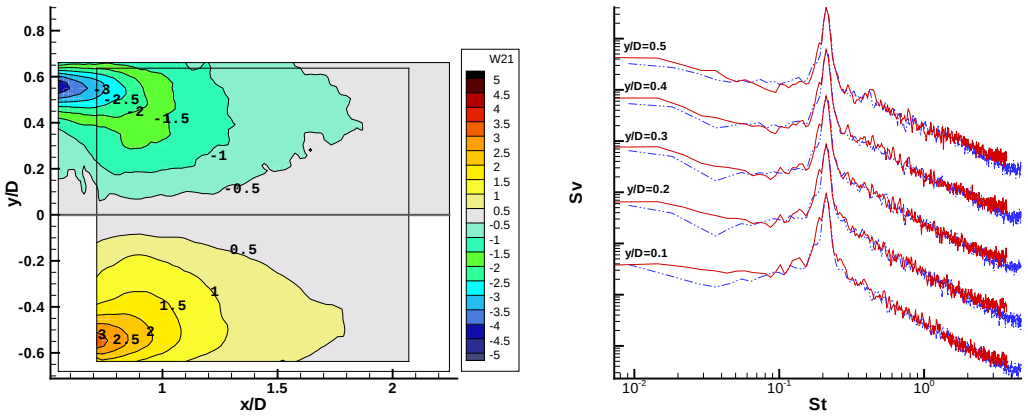

(a) iso contours of Ω_{21} (top: low data rate PIV, bottom: TRPIV)

(b) spectra of v at $x/D = 1$, and different y/D

Figure 1. Comparison of new mesurements with the old measurements

Before presenting results in the following sections, some comparisons between these new TRPIV measurements and the former measurements are necessary, given the small differences in the experimental set-up. First, some comparisons between the TRPIV measurements and the former measurements are made. Figure 1a shows a comparison of the mean $\overline{\Omega_{21}}$ component of the rotation rate tensor. Although not shown here, the recirculation length is found 1.25 and agrees well with the value of 1.28 found with low data rate PIV. Figure 1b shows a comparison of velocity spectra at the same points issue from the new TRPIV measurements, and TRPIV

performed in the S1 wind tunnel. A very good agreement is also achieved. Therefore, the influence of the aspect ratio which had to be modified comparing to the previous studies is found to not have a important effect in the middle span plane.
Some results of a Detached Eddy Simulation, which has been performed on a domain that corresponds precisely to the experimental geometry, are also presented in this paper. This simulation, which have been validated against experiment using time averaging, phase averaging and POD in [12], will be presented in details in a companion paper [8] and the numerical details are not presented here. The data set analysed here consists in 14000 instantaneous snapshots, corresponding to approximately 90 vortex shedding periods, the dimensionless time step being 0.0321.

3. Instantaneous motion

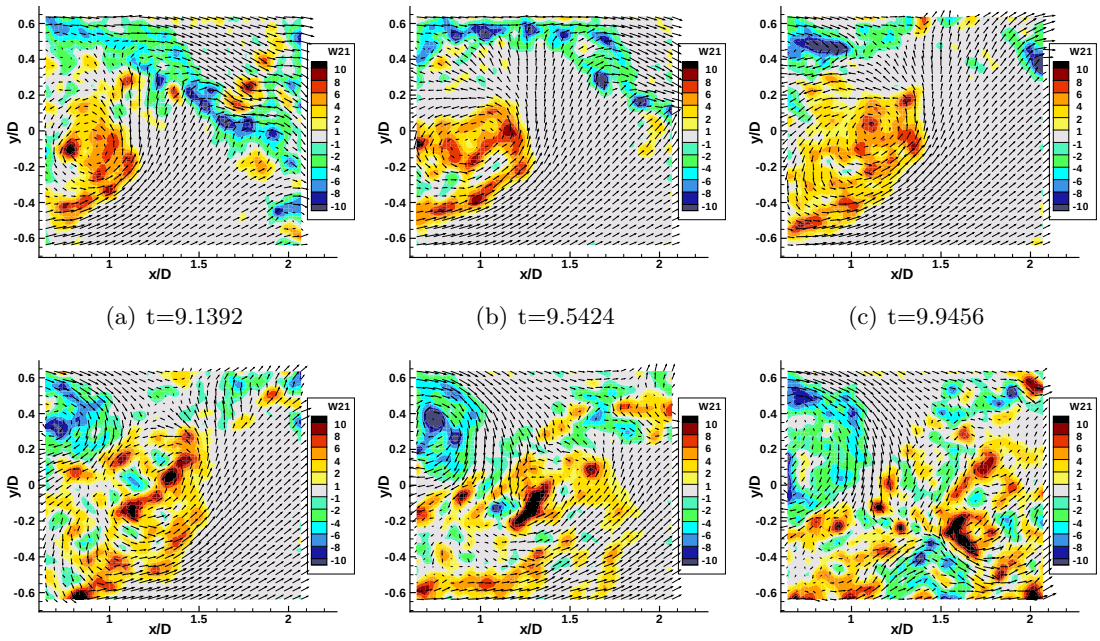

(a) t=9.1392 (b) t=9.5424 (c) t=9.9456

(d) t=10.3488 (e) t=10.752 (f) t=11.1552

Figure 2. Sequence of instantaneous fields (TRPIV)

Figure 2 shows a sequence of instantaneous vorticity and velocity, corresponding approximately to half a period (one picture every three is represented and one velocity vector every two is represented). The vortex shedding is clearly shown, together with smaller vortices in the separated shear layer which are wrapped around the Kármán vortices. This behavior is in good agreement with the measurements of [7] at a lower Reynolds number, although the flow is more irregular, as could be expected at this high Reynolds number.
Regarding the velocity spectra, shown in figure 3 at different locations, they classically exhibit a peak and harmonics which are linked with the vortex shedding, and a continuous part which corresponds to the turbulent motion. As expected, due to the absolute character of the von Kármán instability, the peak which corresponds to the vortex shedding is found at the same dimensionless frequency at every point (Strouhal number St=0.21). On the rear axis, the first harmonic is predominant in

the u spectrum due to the symmetry of the flow. It is also seen that the level of the second harmonic increases as x/D increases, especially for v.

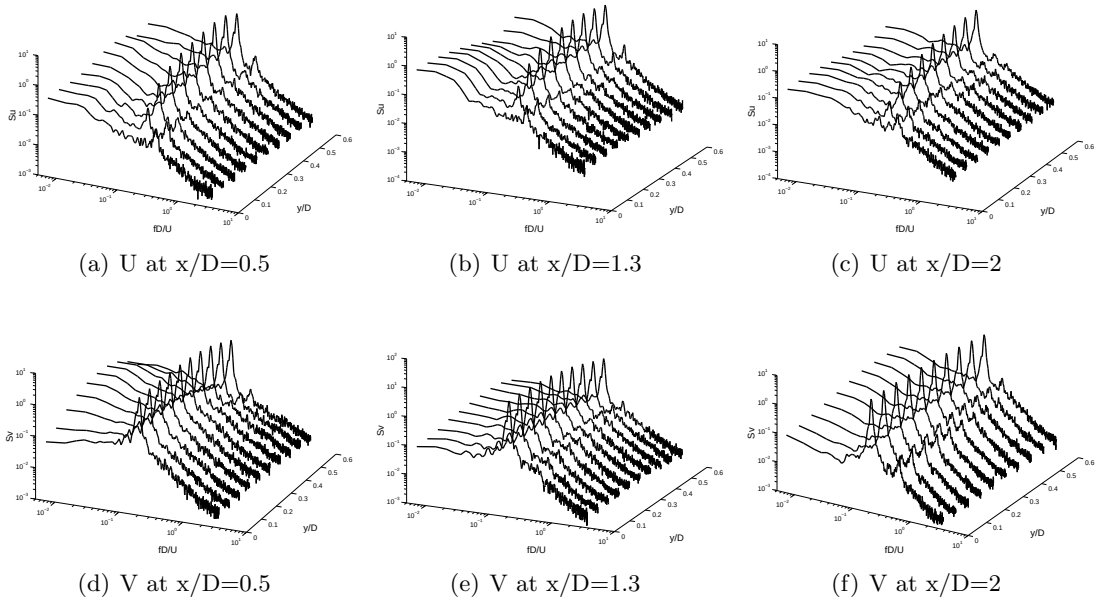

(a) U at x/D=0.5 (b) U at x/D=1.3 (c) U at x/D=2

(d) V at x/D=0.5 (e) V at x/D=1.3 (f) V at x/D=2

Figure 3. Velocity spectra in the near wake (TRPIV)

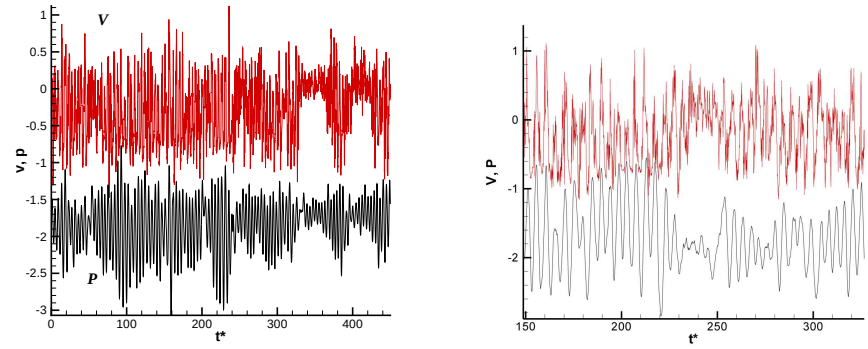

Figure 4. Time signal of V velocity at $x/D = 1$, $y/D = 0.5$ and of the pressure signal at $\theta = 70°$ from the simulation (left) and the experiment (right)

The same temporal behavior has been found in the DES simulation. Looking at the time signals of velocity and pressure obtained from the experiments and the simulation, it also appears that some irregularities are present at certain instants (Fig 4 at $t^* \simeq 350$ and $t^* \simeq 400$ for the DES and $t^* \simeq 240$ for the experiment). During these instants, which do not appear with a regular frequency, the periodic component of the pressure and of the velocity in the very near wake seems to disappear and the 'mean value' of v tends to zero. By looking at the field on a larger domain, it appears that the formation of the vortices occurs further downstream in the wake, the velocity signal at a position further downstream still exhibiting a periodic component (Fig 5).

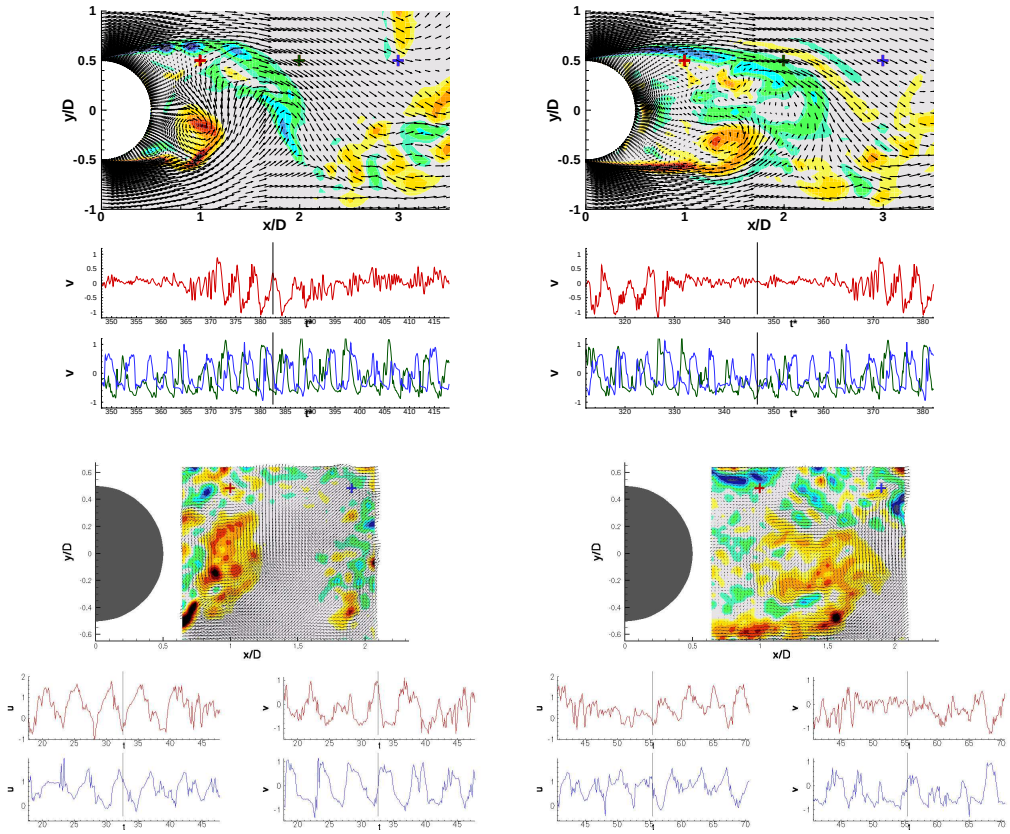

Figure 5. Near wake behavior at instants where the shedding is regular (left) and irregular (right). top: DES, bottom: TRPIV

4. POD and Phase averaging

The quasi periodicity of the vortex shedding allows the use of phase averaging, according to [13], using the triple decomposition:

$$U_i = \overline{U_i} + \tilde{U}_i + u_i' \tag{1}$$

where $\overline{U_i}$ is the time-independent mean flow, $\tilde{U}_i$ is the quasi periodic fluctuating component, u_i' is the random fluctuating component, and $\langle U_i \rangle = \overline{U_i} + \tilde{U}_i$ is the phase averaged velocity.

In [11], this was done using the pressure signal on the cylinder at $\theta = 70°$ as a trigger signal. In [10], it was shown that due to phase lags occurring at certain instants between the pressure signal and the velocity in the wake, a residual periodic component remained in the 'random fluctuation', the spectra of which exhibited a small peak in addition to the continuous part. As a result, the contribution of the coherent motion to the time independent Reynolds stresses was underestimated and that of the random motion was overestimated. To alleviate this problem, the phase angle was then defined using the coefficients associated with the two first POD modes, following [2] and [14]. It was shown that the vortices was less smoothed by the averaging, and that the level of the contribution of the 'random motion' to the time independent Reynolds stresses was diminished. The data used here, which are resolved in space and time, allow to look more precisely at the time evolution of

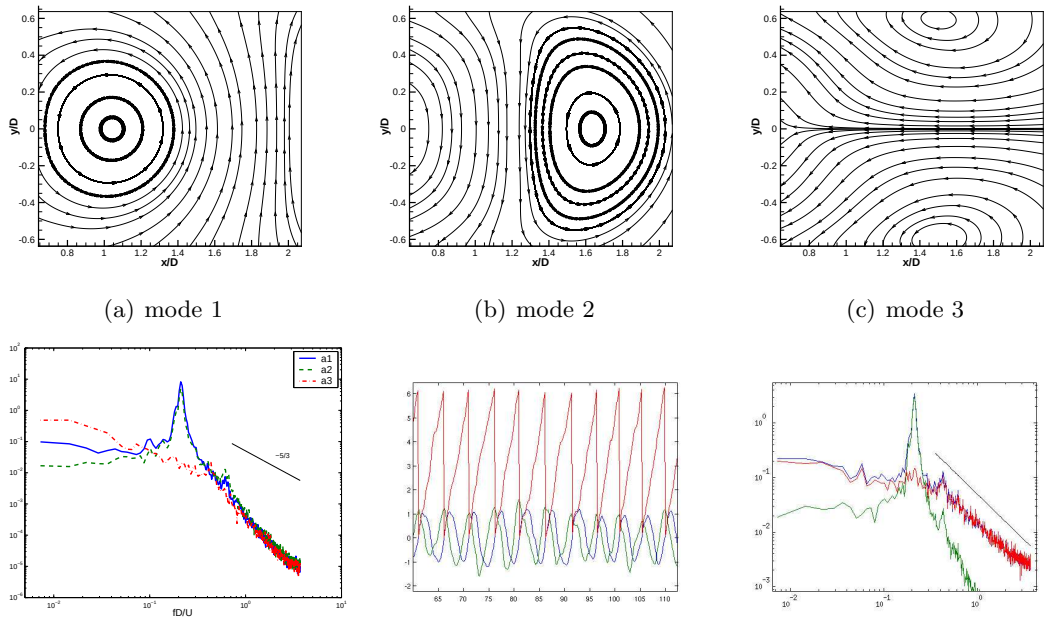

(a) mode 1 (b) mode 2 (c) mode 3

(d) spectra of POD coefficients (e) time evolution of coefficients a_1, a_2 and φ_{POD} (f) spectrum of v, $\tilde{V}$ and v' at $x/D = 1.5$, $y/D = 0.5$

Figure 6. POD and phase averaging (TRPIV)

the POD coefficients, as well as the achieved decomposition from a spectral point of view.

Figures 6a, b, c show the first POD modes, obtained from the TRPIV measurements. In agreement with many other studies in wakes ([9], [3],...), the two first mode are linked with the von Kármán vortices. Spectra of the coefficients associated with these modes are represented in figure 6d. As expected, the spectra of the first two coefficients mainly exhibit a peak at the Strouhal frequency. The spectrum of the third coefficient is more important in the low frequency range. The temporal evolution of the first two coefficients, represented in figure 6e, confirms the possibility to define a phase angle representative of the vortex shedding using:

$$\varphi_{POD} = \arctan\left(\frac{\sqrt{2\lambda_2}}{\sqrt{2\lambda_1}}\frac{a_1}{a_2}\right) \tag{2}$$

where λ_1 and λ_2 are the corresponding eigenvalues. The time evolution of this phase angle is represented on figure 6e. As this phase angle is defined directly from the velocity to be averaged, the effects of the phase lags occurring between the reference signal and the velocity are expected to be alleviated.

For the phase averaging, the instants where the shedding is irregular discussed in the preceding section have been detected and removed. As a low amplitude of the first two POD coefficients is observed during these instants, this was achieved by applying a threshold to $\sqrt{a_1^2 + a_2^2}$. Approximately 20% of the signal was rejected.

Although not shown here, this phase averaging have also been applied to the numerical data, and as simulation give access to the whole domain, the influence of the region on which is performed POD have been studied. It appears that the peak in the spectra are well represented by the two first POD modes when using a region

which is extended up to approximateley $5D$. Taking a larger region leads to obtain more modes linked with the von Kármán vortices, and then it is difficult to define a phase angle. However, the definition of a phase angle when POD is performed in the near wake allows the phase averaging on all the domain, and the results appears similar to those achieved for the experiment.

The resulting phase averaged motion and fluctuation away from this phase average can be view from a spectral point of view. Figure 6f shows spectra of $\tilde{v}$ and v' at $x/D = 1.5$ and $y/D = 0.5$. A significant reduction of the residual peak in the v' spectrum is achieved using POD coefficients, confirming that the effects of phase jitter are alleviated. The same conclusions have been obtained for the simulation.

5. Analysis of phase averaged and turbulent motion

The phase averaged fields and phase averaged turbulent stresses obtained are presented in this section. Figure 7 shows the phase averaged velocity, the $\langle \Omega_{21} \rangle$ component of the rotation rate tensor, the turbulent stresses obtained from 2C-PIV and 3C-PIV, as well as the turbulent kinetic energy and the production term at the phase angle $\varphi = 45°$.

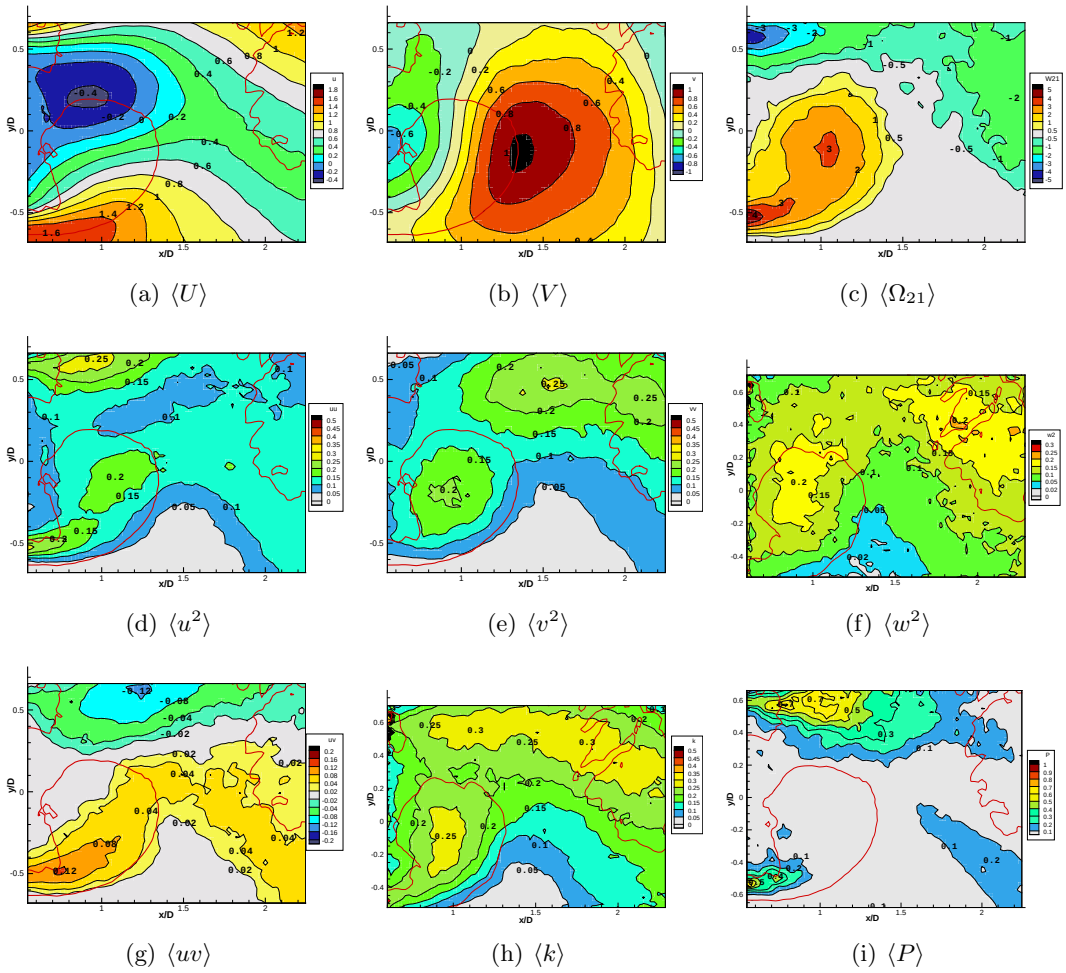

(a) $\langle U \rangle$ (b) $\langle V \rangle$ (c) $\langle \Omega_{21} \rangle$

(d) $\langle u^2 \rangle$ (e) $\langle v^2 \rangle$ (f) $\langle w^2 \rangle$

(g) $\langle uv \rangle$ (h) $\langle k \rangle$ (i) $\langle P \rangle$

Figure 7. Phase averaged quantities at $\varphi = 45°$

$\langle\Omega_{21}\rangle$ clearly exhibits the vortex shedding. The maximum value at the centre of the vortices is of order 3 at $x/D \simeq 1$ during their formation and decreases to 2 at $x/D \simeq 2$ at the beginning of their convection. $\langle u^2\rangle$ and $\langle uv\rangle$ presents their highest values in the shear regions near the separation. When the vortices are formed, the two lobes of high values of $\langle u^2\rangle$ are transported towards the rear axis, and the centre of the vortices. At the beginning of the convection, the highest values of $\langle uv\rangle$ are located in the shear regions near the saddles points between the vortices, where the deformation rate is important. Concerning the normal stresses in the near wake, they all exhibit their highest values near the centre of the vortices when they begin to be convected. High values of $\langle v^2\rangle$ and $\langle w^2\rangle$ are also present between the vortices, and can be supposed to be linked with the presence of longitudinal vortices connecting the primary one. Finally, regions of low values of stresses are identified in front of the vortices, corresponding to external fluid entering in the wake. It is also noticeable that a strong anisotropy is observed. The general topology of the stresses is found in good agreement with precedent studies in wakes ([1], [6], [4],...). With the use of stereoscopic PIV, the turbulent kinetic energy can be evaluated without assumption on $\langle w^2\rangle$, and its topology is compared here to the production term that appears in its equation. It appears, in agreement with the aforementionned studies, that while the production is mainly located near the saddles points in the shear regions, where the deformation rate and $\langle uv\rangle$ are important, the turbulent kinetic energy is mainly located near the centre of the vortices, suggesting a transport of the turbulent energy.

6. Conclusion and Outlooks

The very near wake of a circular cylinder at high Reynolds number was experimentally studied using PIV, stereoscopic PIV and TRPIV. Due to the organised and random character of the flow, a particular attention was paid to achieve a decomposition of the motion into a coherent and a turbulent part. While it was shown in precedent studies that phase averaging using the pressure signal on the cylinder could lead to an overestimation of the random motion, due to phase lags occurring between the reference signal and the velocity in the wake, it has been shown that the first POD coefficients could be used to define a phase angle directly from the velocity fields, then alleviating the overestimaion of the turbulent motion. Two complementary data sets which are revolved in space and time, obtained by TRPIV and by a DES simulation, have been used to analysed the instantaneous motion, as well as to analyse the POD and phase averaging that were performed. Then, a cartography of the phase averaged mean motion and turbulent stresses in the near wake have been provided.
A future study will be devoted to the analysis of the tridimensionality, and particularly the longitudinal vortices which connect the primary ones, using both the presented numerical results and also Time Resolved Stereoscopic measurements in planes along the spanwise direction.

Acknowledgements

The authors acknowledge the partial funding of the work presented here by the European Community during the DESider project (in the 6^{th} Framework Program,

under Contract No. AST3-CT-2003-502842) and by the German Research Foundation (DFG) within the scope of the Collaborative Research Center SFB 557.

References

[1] B. Cantwell and D. Coles. An experimental study of entrainment and transport in the turbulent near wake of a circular cylinder. *J. Fluid Mech.*, 136:321–374, 1983.

[2] M. Ben Chiekh, M. Michard, N. Grosjean, and J. C. Bera. Reconstruction temporelle d'un champ aéodynamique instationnaire partir de mesures PIV non résolues dans le temps. In 9^e *Congrès Francophone de Vélocimétrie Laser*, 2004.

[3] A. E. Deane, I. G. Kevrekidis, G. E. Karniadakis, and S. A. Orzag. Low-dimensional models for complex geometry flows: Application to grooved channels and circular cylinders. *Phys. Fluids A*, 3:2337–2354, 1991.

[4] A. K. M. F. Hussain and M. Hakayawa. Eduction of large-scale organized structures in a turbulent plane wake. *J. Fluid Mech.*, 180:193–229, 1987.

[5] B. Lecordier and M. Trinite. Advanced PIV algorithms with image distortion - Validation and comparison from synthetic images of turbulent flows. In *PIV03 Symposium*, Busan, Korea, 2003.

[6] A. Leder. Dynamics of fluid mixing in separated flows. *Phys. Fluids A*, 3(7):1741–1748, 1991.

[7] A. Leder and M. Brede. Comparisons between 3D-LDA measurements and TR-PIV data in the separated flow of a circular cylinder. In 12^{th} *Int. Symp. on Applications of Laser Techniques to Fluid Mechanics*, Lisbon, Portugal, 2004.

[8] C. Mockett, R. Perrin, T. Reimann, M. Braza, and F. Thiele. Analysis of detached-eddy simulation for the flow around a circular cylinder with reference to piv data. In *IUTAM Symposium on Unsteady Separated Flows and their Control, June 18-22*, Corfu, Greece, 2007.

[9] B. Noack, K. Afanasiev, M. Morzynski, G. Tadmor, and F. Thiele. A hierarchy of low-dimensional models for the transient and post-transient cylinder wake. *J. Fluid Mech.*, 497:335–363, 2003.

[10] R. Perrin, M. Braza, E. Cid, S. Cazin, A. Barthet, A. Sevrain, C. Mockett, and F. Thiele. Phase averaged turbulence properties in the near wake of a circular cylinder at high Reynolds number using POD. In 13^{th} *Int. Symp. on Applications of Laser Techniques to Fluid Mechanics*, Lisbon, Portugal, 2006.

[11] R. Perrin, E. Cid, S. Cazin, A. Sevrain, M. Braza, F. Moradei, and G. Harran. Phase averaged measurements of the turbulence properties in the near wake of a circular cylinder at high Reynolds number by 2C-PIV and 3-C PIV. *Experiments in Fluids*, 42(1), 2007.

[12] R. Perrin, C. Mockett, M. Braza, E. Cid, S. Cazin, A. Sevrain, P. Chassaing, and F. Thiele. Joint numerical and experimental investigation of the flow around a circular cylinder at high reynolds number. *Topics in Applied Physics, PIVNET 2. To be published*, 2007.

[13] W. C. Reynolds and A. K. M. F. Hussain. The mechanics of an organized wave in turbulent shear flow. Part 3. Theoretical models and comparisons with experiments. *J. Fluid Mech.*, 54:263–288, 1972.

[14] B. W. van Oudheusden, F. Scarano, N. P. van Hinsberg, and D. W. Watt. Phase-resolved characterization of vortex shedding in the near wake of a square-section cylinder at incidence. *Experiment in Fluids*, 39:86–98, 2005.